PHYSICAL REVIEW B **90**, 094204 (2014)

Structure of molten titanium dioxide

O. L. G. Alderman,[1,2,*] L. B. Skinner,[1,2,3] C. J. Benmore,[2] A. Tamalonis,[1] and J. K. R. Weber[1,2]
[1]*Materials Development, Inc., Arlington Heights, Illinois 60004, USA*
[2]*X-Ray Science Division, Advanced Photon Source, Argonne National Laboratory, Argonne, Illinois 60439, USA*
[3]*Mineral Physics Institute, Stony Brook University, Stony Brook, New York 11794-2100, USA*

(Received 29 July 2014; revised manuscript received 27 August 2014; published 18 September 2014)

The x-ray structure factor of molten TiO_2 has been measured, enabled by the use of aerodynamic levitation and laser beam heating, to a temperature of $T = 2250(30)$ K. The Ti-O coordination number in the melt is close to $n_{TiO} = 5.0(2)$, with modal Ti-O bond length $r_{TiO} = 1.881(5)$ Å, both values being significantly smaller than for the high temperature stable rutile crystal structure ($n_{TiO} = 6.0$, $r_{TiO} = 1.959$ Å). The structural differences between melt and crystal are qualitatively similar to those for alumina, which is rationalized in terms of the similar field strengths of Ti^{4+} and Al^{3+}. The diffraction data are used to generate physically and chemically reasonable structural models, which are then compared to the predictions based on various classical molecular dynamics (MD) potentials. Interatomic potentials, suitable for modeling molten TiO_2, are introduced, given the inability of existing MD models to reproduce the diffraction data. These potentials have the additional advantage of being able to predict the density and thermal expansion of the melt, as well as solid amorphous TiO_2, in agreement with published results. This is of critical importance given the strong correlation between density and structural parameters such as n_{TiO}. The large thermal expansion of the melt is associated with weakly temperature dependent structural changes, whereby simulations show that $n_{TiO} = 5.85(2) - [3.0(1) \times 10^{-4}]T$(K, 2.75 Å cutoff). The TiO_2 liquid is structurally analogous to the geophysically relevant high pressure liquid silica system at around 27 GPa. We argue that the predominance of fivefold polyhedra in the melt implies the existence of as-yet-undiscovered TiO_2 polymorphs, based on lower-than-octahedral coordination numbers, which are likely to be metastable under ambient conditions. Given the industrial importance of titanium oxides, experimental and computational searches for such polymorphs are well warranted.

DOI: 10.1103/PhysRevB.90.094204 PACS number(s): 61.43.−j, 61.05.cp, 61.20.Ja

I. INTRODUCTION

Titanium dioxide (TiO_2) is an extensively studied photocatalytic material [1] which can be used for solar energy conversion, water splitting, and degradation of organic industrial pollutants [2]. TiO_2 is known to demonstrate flash sintering [3–5], that is, sintering at relatively low furnace temperatures under the application of an electric field. Oxygen deficient TiO_{2-x} represents a physical realization of a memristive device [6–9]. These phenomena are all related to charged defect formation in TiO_2 and/or to the formation of Ti_nO_{2n-1} Magnéli phases. Knaup *et al.* [10] have recently raised the possibility of a liquid intermediate phase in both memristive device operation and during flash sintering, presumably in the form of *local* melting. Narayan [4] has proposed a mechanism for flash sintering which does indeed involve local melting at grain boundaries. The structure and properties of TiO_2 rich melts are also important for understanding industrial smelting of ores, e.g., ilmenite ($FeTiO_3$) [11], and in the direct electrochemical reduction of melts [12,13], e.g., for extraterrestrial resource generation.

TiO_2 is an end-member to several important mixed oxide systems, such as BaO-TiO_2, which includes the archetypal ferroelectric $BaTiO_3$, and such crystals are often derived from the liquid state, from either stoichiometric melts or fluxes. TiO_2 is often used as a component in melt-derived mixed oxide glasses to increase refractive index [14] or as a nucleating agent in glass-ceramics [15,16]. In terms of glass formation, TiO_2 is an intermediate oxide, or conditional glass former, partaking in network formation while typically not capable of being melt-quenched to form glass itself. Amorphous TiO_2 films have been obtained by various methods [17], such as reactive evaporation and deposition. In mixed oxide glasses, Ti is often found in fivefold coordination, including unusual $[TiO_{4+1}]$ ($BaTi_2O_5$ [18]) and $[TiO_{1+4}]$ ($K_2O \cdot TiO_2 \cdot 2SiO_2$ [19]) polyhedra, while in amorphous TiO_2, Ti is found to have an average coordination number lying between five and six [20] (dependent upon growth method). TiO_2 is strongly polymorphic, with at least five forms known to be metastable with respect to rutile under ambient conditions (Fig. 1), and several high pressure polymorphs also exist [21]. All ambient pressure polymorphs, as well as the substoichiometric Magnéli phases, contain Ti within $[TiO_6]$ octahedra [22], although recent structural refinements have been used to show that one Ti site in the TiO_2(B) polymorph may be considered as fivefold coordinated to oxygen [23]. The octahedral environment is also the most common in mixed oxide titanates (e.g., $BaTiO_3$), but several examples exist which contain $[TiO_4]$ tetrahedra (e.g., Ba_2TiO_4 [24,25]), and indeed fivefold polyhedra (e.g., β-$BaTi_2O_5$ [18]).

Recently, a trend for reduced cation-oxygen coordination in oxide melts and glasses, compared to their crystalline counterparts, has been observed [26]. The effect is typically larger for lower field strength cations, and Ti^{4+} has a similar field strength to Al^{3+}, for which there is a large drop in average coordination number, from 6.0 to 4.4 in molten alumina [27–29], upon melting the stable corundum form. In the case of Al_2O_3, several other crystalline polymorphs exist, within which Al exists in both tetrahedral and octahedral

---

[*] oalderman@gmail.com

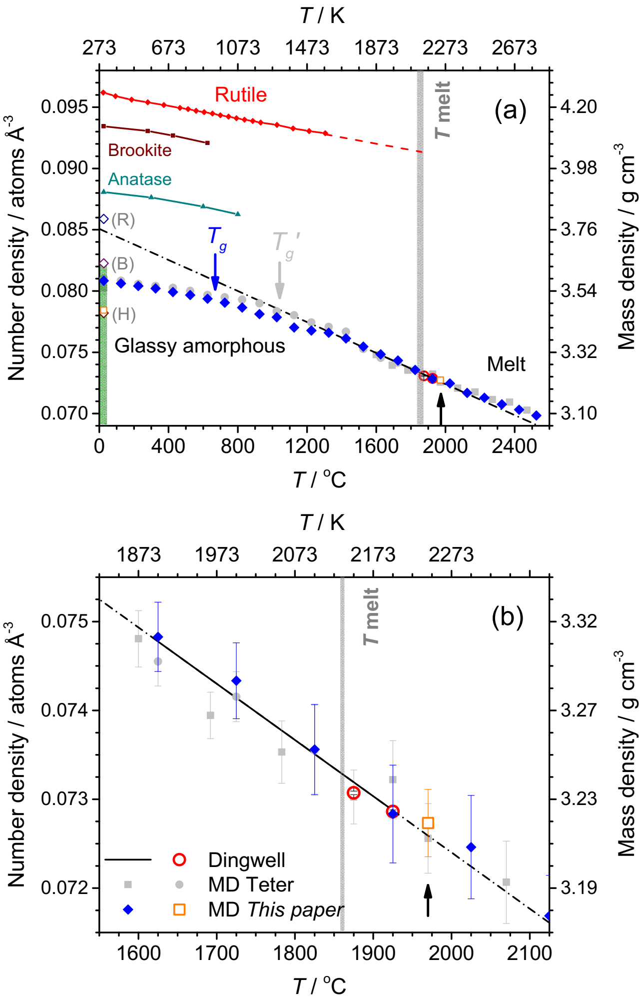

FIG. 1. (Color online) (a) Experimental temperature dependence of the densities of rutile [55], brookite [86], anatase [87], and liquid [39] TiO_2 (open red circles). The solid black line is the trend derived by Dingwell [39], and its extrapolation is shown as a broken dash-dot curve. The rutile trend is extrapolated (dashed curve) up to the melting point (vertical gray bar). Points denoted (R), (B), (H), respectively, show the room temperature densities of ramsdellite [88], beta- [89], and hollandite [90] TiO_2. The vertical green bar plots the range of room temperature densities of amorphous TiO_2 thin films obtained by Mergel *et al.* [17]. Densities of liquid and amorphous TiO_2 obtained by MD modeling using the potentials derived in this paper are shown as closed (blue) diamonds and open (orange) squares, and using the modified Teter potentials; closed (gray) squares and circles (quench). Glass transition temperatures are indicated as T_g and T_g', respectively. The vertical black arrow indicates the temperature of the x-ray diffraction measurement (this paper). (b) A close up around the melting point. Error bars are standard deviations.

coordination to oxygen [30]. Therefore, if TiO_2 were to exhibit a drop in coordination number from 6.0 upon melting, as predicted by recent observations [26], it can be argued that new metastable polymorphs of TiO_2, based on lower-than-octahedral Ti coordination, may be realized under suitable conditions.

Finally, molten TiO_2 potentially represents a useful structural analog to high pressure SiO_2 and GeO_2 melts, with the structure and properties of liquid silica under pressure, in particular, bearing significant geophysical importance.

We present here structural measurements on the highly refractory liquid TiO_2, at a temperature of 2250(30) K, using a combination of aerodynamic levitation, CO_2 laser beam heating, and synchrotron x-ray diffraction. The measurement is used to assess the high temperature applicability of several interatomic potential parameterizations used in classical molecular dynamics (MD) modeling, to improve upon these, and to model the temperature dependence of the liquid and amorphous state densities (thermal expansions) and structures.

II. THEORY

In a scattering experiment, the x-ray structure factor, $S(Q)-1$, is related to the measured differential x-ray scattering cross-section, $d\sigma(Q)/d\Omega$, by [31]

$$S(Q)-1 = \left[\frac{d\sigma}{d\Omega}(Q) - \sum_i c_i f_i^2(Q) - \sum_i c_i C_i(Q)\right]\left[\sum_i c_i f_i(Q)\right]^{-2}, \tag{1}$$

where c_i is the atomic faction of element i, $f_i(Q)$ the x-ray atomic form factor, and $C_i(Q)$ the Compton scattering contribution. $Q = (4\pi \sin\vartheta)/\lambda$ is related to the scattering angle 2ϑ and the x-ray wavelength λ. Written in terms of the partial structure factors, $S_{ij}(Q)-1$, between pairs of atoms i-j,

$$S(Q)-1 = \left\{\sum_{i,j} c_i c_j f_i(Q) f_j(Q)[S_{ij}(Q)-1]\right\}\left[\sum_i c_i f_i(Q)\right]^{-2}, \tag{2}$$

and we may define the pair weighting factors

$$W_{ij}(Q) = [(2-\delta_{ij})c_i c_j f_i(Q) f_j(Q)]\left[\sum_i c_i f_i(Q)\right]^{-2}, \tag{3}$$

with δ_{ij} the Kronecker delta. $S(Q)-1$ is related by sine Fourier transform to the total correlation function

$$T(r) = 4\pi\rho r + \frac{2}{\pi}\int_0^{Q_{\max}} Q\,[S(Q)-1]\,M(Q)\sin(rQ)dQ, \tag{4}$$

where r is the scalar interatomic distance, ρ is the atomic number density, and $M(Q)$ is the Lorch modification function [32], chosen to reduce the effects of the finite limits ($0 < Q \leqslant Q_{\max}$) of the integral which are used in practice. The partial pair correlation functions, $t_{ij}(r) = 4\pi\rho c_j r g_{ij}(r)$, can be obtained using Eq. (4) and making the substitutions $T(r) \to t_{ij}(r)$, $\rho \to \rho c_j$ and $S(Q) \to S_{ij}(Q)$. Since the present high energy x-ray measurements are far from Ti and O absorption edges, dispersion terms in $f_i(Q)$ are neglected.

III. METHODS

A. Diffraction measurements

Diffraction measurements on liquid TiO_2 were performed at beamline 11-ID-C [33] of the Advanced Photon Source (Argonne, Illinois, USA). A spheroidal sample approximately 3 mm in diameter was levitated in a stream of argon (99.999% pure) flowing through a converging-diverging aerodynamic nozzle. The sample was heated from above with a partially focused CO_2 laser beam. The incident heating power was adjusted to control the sample temperature, which was measured with a single color pyrometer (Chino model IRCS) sighted onto the top of the sample where it was also being heated. The apparent temperature was corrected using a Wien's displacement law approximation [34] with a spectral emissivity value of 0.87 for the molten TiO_2 at the pyrometer wavelength of 0.85 μm. The emissivity value was estimated from the Fresnel losses for a material with a refractive index of 2.1, which is the value appropriate to amorphous TiO_2 [17] at the density of the melt. The pyrometer temperature was also corrected for reflection losses from a window and lens that were in the optical path. The temperature correction amounts to 86 K at the apparent measurement temperature of 2168 K, and we estimate a true temperature of 2250(30) K, with the uncertainty arising from estimated temperature gradients and fluctuations, in addition to the emissivity correction. Although there are top-to-bottom temperature gradients on the order of 100 K throughout the sample, by making both temperature and x-ray measurements at the top where it is heated, the temperature of the liquid being probed is relatively uniform. Structure was measured using a high energy (111.16 keV) x-ray beam with cross-section $200\,\mu\text{m} \times 400\,\mu\text{m}$ horizontally incident upon the top of the sample in the region where it was heated.

The chamber housing the nozzle was open to the atmosphere at its top where the laser beam entered, while the incident and scattered x rays passed through thin kapton windows. An area x-ray detector (Perkin Elmer XRD1621, 2048×2048 pixels of $200\,\mu\text{m} \times 200\,\mu\text{m}$ Tl-doped CsI) was used with several offsets perpendicular to the beam, and the patterns averaged together during the data reduction to reduce any effects due to trapped excited states [35]. Sample-to-detector distance (394 mm) was calibrated using a polystyrene bead coated in polycrystalline CeO_2 powder, which was placed in the nozzle.

To obtain samples suitable for levitation, TiO_2 (Aldrich, 99.99%) was premelted in a water-cooled copper hearth, open to the atmosphere, using a 100 W CO_2 laser, and the surface tension of the melt relied upon to form roughly spherical beads. Sample contamination has been shown to be negligible by this method [36]. Discoloration of the material from white to dark gray was observed, revealing at least a small reduction in oxidation state (Ti^{4+} to Ti^{3+}). However, mass measurements on batches of up to 122 mg could not resolve any mass loss, and a final formula TiO_{2-x} with $x = 0.00(2)$, equivalent to an oxygen deficiency of 1% or less. The TiO_2 melt was somewhat unstable during levitation, and only short measurements were possible. The x-ray diffraction result shown here is averaged from frames collected over a total of 150 s.

To obtain information on the recovered material, separate experiments were performed at beamline 6-ID-D of the Advanced Photon Source on several finely powdered recovered beads. This was necessary due to the presence of strong preferred crystallite orientation in the solidified bead in the levitation nozzle. Powder was held within vertical, thin-walled (100 μm) kapton tubes of 2 mm internal diameter. Here, 86.41 keV x-rays, and two separate sample-to-detector distances of 294 and 1104 mm were used, the latter yielding higher Q-space resolution.

The raw data were reduced from two-dimensional images and corrected [35] for the effects of polarization, absorption, geometry, and normalized using the programs Fit2d and PDFgetX2 [37] (GudrunX [38] was also used as a consistency check).

B. Liquid density

The density of liquid TiO_2 has been measured by Dingwell [39] who obtained the linear relation $\rho(T) = 3.8375 - (2.8 \times 10^{-4})T$ (in Kelvin and grams per cubic centimeter). This trend is shown in Fig. 1 and was obtained from two temperature points [39] plus an extrapolation to supercooled TiO_2 at 1873 K from $CaSiO_3$-TiO_2 pseudobinary melts containing up to 80 mol% TiO_2 [40]. Extrapolating the Dingwell function to 2250 K gives a liquid density of $3.21\,\text{g}\,\text{cm}^{-3}$ (0.0725 atoms Å^{-3}), which we use for our analysis.

C. Empirical potential structure refinement

Empirical potential structure refinement (EPSR) [41] has been used to obtain a physically and chemically reasonable liquid structure, by construction, in excellent agreement with the measured x-ray structure factor and melt density. Although not unique, the EPSR model provides an estimate of the atomic structure and partial structure factors and serves as a basis for comparison to MD predictions. Initial Monte Carlo simulations were performed on 1032 atoms held within a cubic box of edge length 24.2 Å set to reproduce the estimated liquid density [39] of $3.210\,\text{g}\,\text{cm}^{-3}$. Atoms interacted via Lennard-Jones (L-J) 12-6 and partial (0.5 e) charge Coulomb terms, smoothly truncated, as described by Soper [41], using a cutoff of 12 Å. The L-J parameters for oxygen were taken from Alderman *et al.* [42] ($\varepsilon_{\text{O}} = 0.92\,\text{kJ}\,\text{mol}^{-1}$ and $\sigma_{\text{O}} = 3.16$ Å) and those for Ti set to $\varepsilon_{\text{Ti}} = 2.23\,\text{kJ}\,\text{mol}^{-1}$ and $\sigma_{\text{Ti}} = 1.31$ Å, so as to approximately reproduce the Ti-O peak of the measured x-ray correlation function. The L-J well depths and radii follow from the Lorentz-Berthelot mixing rules: $\varepsilon_{ij} = (\varepsilon_i \varepsilon_j)^{1/2}$ and $\sigma_{ij} = (\sigma_i + \sigma_j)/2$. Once equilibrated using the reference potentials, the empirical potential was permitted to become finite and iteratively modified in order to achieve agreement with the measured x-ray structure factor.

D. Molecular dynamics

Classical MD simulations were performed using the DLPOLY [43] code. Many interatomic potential parameterizations for titanium-oxygen systems exist in the literature, and we test here only the most recent or relevant. The only published simulations of liquid TiO_2 were made by Hoang [44,45], using the potentials of Matsui and Akaogi (MA) [46], which were those recommended after a review by Collins *et al.* [47] of the existing potentials at the time (1996). We also assess the more

TABLE I. Parameters for the various interatomic potentials used [Eqs. (5) and (6)] for MD simulations of TiO_2. The three Teter parameters that were modified are italicized (see main text). The final column gives the approximate density derived after simulation in the *NPT* ensemble at 1 atm and 2243 K.

Potential	f	Pair ij	A_{ij} (eV)	B_{ij} (Å^{-1})	σ_{ij} (Å)	C_{ij} (eV Å^{-6})	D_{ij} (eV Å^{-8})	*NPT* ρ (g cm^{-3})
MA	0.549	Ti-O	78.316 76	5.154 639	2.8162	117 229.7	0	1.4
		O-O	1319.193	4.273 504	3.2678	281 351.2	0	
Teter	0.6	Ti-O	237 07.91	5.388 512	0	14.513	0	2.9
		O-O	1844.746	2.909 98	0	192.58	0	
Modified Teter	0.6	Ti-O	237 07.91	5.388 512	0	14.513	*1.28*	3.2
		O-O	*1881.641*	2.909 98	0	192.58	*112*	
This paper	0.6	Ti-O	2963.489	4.028 794	0	14.513	− 2.75	3.2
		O-O	2213.910	2.909 98	0	192.58	−106	
		Ti-Ti	180 00.00	4.0	0	800.00	−500	
			E_{ij} (eV)	k_{ij} (Å^{-1})	r_{ij} (Å)			
Pedone	0.6	Ti-O	0.024 235	2.254 703	2.708 943			2.6
		O-O	0.042 395	1.379 316	3.618 701			

recent potentials of Pedone *et al.* (Pedone hereafter) [48] and the rigid ion potentials of Teter [49], the latter of which are unpublished, but have been used extensively in the literature, particularly for the simulation of silicate glasses [49,50] and melts [51,52] (often with minor modifications). Both the MA and Teter pair potentials can be recast in the form

$$U_{ij}(r) = A_{ij}\exp[B_{ij}(\sigma_{ij} - r)] - \frac{C_{ij}}{r^6} - \frac{D_{ij}}{r^8} + f^2e^2\frac{q_iq_j}{4\pi\varepsilon_0 r}, \tag{5}$$

where q_i are formal ionic charges in units of the electron charge e, $f \leqslant 1$ is a charge scaling factor which is reduced from unity in order to simulate partial covalency, and ε_0 is the permittivity of free space. The parameter values used are given in Table I. The Pedone potentials are of the Morse form

$$U_{ij}(r) = E_{ij}(\{1 - \exp[-k_{ij}(r - r_{ij})]\}^2 - 1) + f^2e^2\frac{q_iq_j}{4\pi\varepsilon_0 r}, \tag{6}$$

and again the parameter values are given in Table I. Note that the full MA potentials include nonzero dispersion and repulsion terms between Ti-Ti pairs; however, we found that neglecting these terms made negligible difference to the resulting structure and so, as for the other models, Ti-Ti pairs interacted only via the repulsive Coulomb term. We also tested the potentials of le Roux and Glasser [53], but these were rejected early on because of the resulting first Ti-O peak in $g_{\mathrm{TiO}}(r)$ being much too sharp as compared to the diffraction data (and to the other MD models). Starting configurations of 4800 atoms were obtained by Monte Carlo simulation using the L-J plus Coulomb potentials introduced in the EPSR section above, with a fixed density of 3.210 g cm^{-3}. The MD simulations were conducted either in the canonical (constant number, volume, temperature [*NVT*]) or the isothermal-isobaric (constant number, pressure, temperature [*NPT*]) ensemble, using a Hoover-Nosé thermostat or thermostat-barostat, typically at $T = 2243$ K and $P = 1$ atm. A time step of 1.0 fs was selected, with the first 1000 MD steps used for equilibration, and particle trajectories typically integrated over a further 49 000 steps. The MA, Teter, and Pedone potentials were all found to result in very low system densities in the *NPT* ensemble, as shown in Table I, with the Teter potentials resulting in the closest density to the expected 3.210 g cm^{-3}. In order to obtain the correct system density, the Teter potentials were softened by adding small attractive $-D_{ij}/r^8$ terms, and increasing the A_{OO} parameter, to which density is extremely sensitive, by 2%. These changes resulted in the modified Teter potentials, Table I. Although the modifications are by no means unique, they are small, result in negligible structural changes at a given density, and most importantly, allow for the prediction of the system density as a function of T and P. A new set of potentials, referred to as those of this paper (Table I) were derived (by heavy modification of the Teter potentials) in order to improve the agreement between simulated and measured x-ray structure factors, while also reproducing existing density data. The A_{TiO} parameter was initially greatly reduced, while also reducing B_{TiO} to maintain the Ti-O peak bond length at the position measured by x-ray diffraction. Non-Coulombic Ti-Ti interaction parameters were then introduced to broaden the Ti-Ti nearest neighbor peak and were adjusted iteratively, along with the density sensitive A_{OO} parameter. Repulsive short-range D_{ij}/r^8 terms were added to remove the unphysical short-range attraction which arises from the Buckingham potential terms. Densities derived from *NPT* simulations at different temperatures are shown in Fig. 1. In addition to MD simulations obtained from the identical (3.210 g cm^{-3}) starting configuration, with various target temperatures (gray squares, Fig. 1), a stepwise quench from 2198 K was also performed (gray circles, Fig. 1). In this case (again in the *NPT* ensemble), the temperature was lowered in 100 K steps down to 298 K, with 1000 equilibration and 24 000 time steps at each T point, resulting in an average cooling rate of 4×10^{12} Ks^{-1}. In the case of the potentials of this paper (see Table I), a starting temperature of 2798 K and 1500 atoms were used for an otherwise identical stepwise quench (blue diamonds, Fig. 1).

IV. RESULTS

The measured liquid structure factor is shown in Fig. 2(a), and is compared to that for the powdered recovered material.

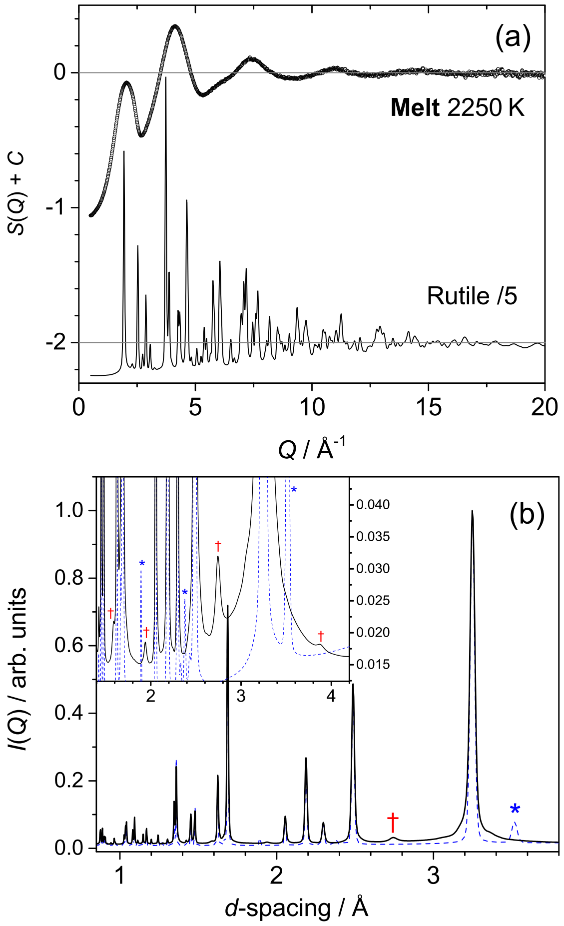

FIG. 2. (Color online) (a) Structure factors $S(Q)$ for liquid (2250 K) and recovered rutile TiO_2, the latter has been divided by a factor 5, and constant offsets C applied, for clarity. (b) Higher resolution (see main text) diffraction patterns $I(Q)$ for starting material (dashed blue curve) and recovered material (solid black curve) as functions of interplanar spacing $d = 2\pi/Q$. Asterisks (*) denote an anatase impurity in the predominantly rutile starting material, while daggers (†) denote unmatched Bragg peaks of a phase impurity in the predominantly rutile recovered material.

Figure 2(b) shows the higher resolution powder diffraction pattern obtained on the room temperature material, which closely matches the expected pattern for rutile TiO_2. This is consistent with the zero mass loss measured, within uncertainty, and the <1% oxygen deficiency thus inferred. The inset [Fig. 2(b)] reveals the presence of a very small phase impurity which could not be indexed according to any of the known TiO_2 polymorphs, or the substoichiometric Magnéli phases, or indeed any known compound within the Ti-O phase diagram. It is possible that the unmatched Bragg peaks belong to a Ti_nO_{2n-1} Magnéli phase with $n > 9$, or to an unknown modification of TiO_2. The powder pattern of the starting material [rutile with anatase impurity, Fig. 2(b)] serves to illustrate the peak broadening evident in the recovered material, arising from rapid solidification and resultant small crystallite sizes, although it is possible that the shoulders on the rutile (110) peak at $d = 3.25$ Å arise due to additional peaks from the unidentified phase impurity.

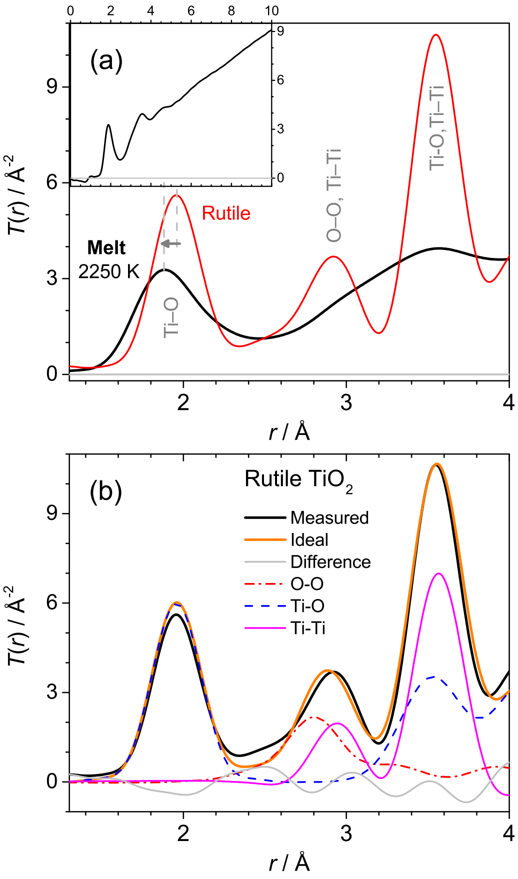

FIG. 3. (Color online) (a) Total correlation functions $T(r)$ for the melt at 2250(30) K and the recovered rutile TiO_2 at room temperature. Inset: $T(r)$ for the melt over an extended r range. (b) Comparison of measured and ideal rutile TiO_2 $T(r)$, also showing the partial pair functions calculated using the XTAL program [91] from the known crystal structure [92].

The short-range structure, as evidenced by the $T(r)$ in Fig. 3(a), differs significantly between crystalline rutile and the TiO_2 melt. Most markedly the first peak, arising due to Ti-O interatomic separations, shifts to shorter distance and reduces in area, both features indicative of a reduced Ti-O coordination number in the melt. Suitable integration of the function $r.T(r)$, Fourier transformed from the modified $S(Q) - 1$, with the Ti-O weighting $[W_{\mathrm{TiO}}(Q)]$ divided out, yields a Ti-O coordination number of 5.0(2), with the peak (modal) bond-length 1.881(5) Å. The integration limits were 1.42 to 2.44 Å, the latter being the position of the first minimum to higher r after the peak. Note however that $T(r)$ does not fall to zero at this minimum, there being a large overlap with other (O-O, Ti-Ti) correlations, and therefore the minimum in $T(r)$ may not correspond to a minimum in the partial $t_{\mathrm{TiO}}(r)$, resulting in an uncertainty which is difficult to quantify from x-ray diffraction alone. As such, it is necessary to generate models in order to aid interpretation of the data. Nonetheless, the average value of $n_{\mathrm{TiO}} = 5.0(2)$ represents an *upper bound* (for the given cutoff), and so the reduction of n_{TiO} in the melt, below the value of 6 in all known crystalline phases of TiO_2 is clear. This is supported by the reduced peak position of 1.881(5) Å (*cf.* 1.962(5) Å in rutile, Table II) which is consistent with fivefold units $[TiO_5]$

TABLE II. Average Ti-O coordination numbers n_{TiO} obtained from x-ray diffraction data on the TiO_2 melt (integration up to the minimum at 2.44 Å) at 2250(30) K, recovered rutile TiO_2 (peak fit), and from the rutile crystal structure [92]. Peak (modal) bond lengths r_{TiO} are also given. The corresponding values obtained from $g_{\mathrm{TiO}}(r)$ for the melt from different MD models and from EPSR are also given, where the second column gives the quality-of-fit parameter $R\chi$ [for $r_{k,\max} = 10$ Å, Eq. (7)], and the fourth the n_{TiO} obtained by integration up to the first minimum of $g_{\mathrm{TiO}}(r)$ at 2.75 Å. Uncertainties are in parentheses.

		n_{TiO}		
	$R\chi$ (%)	$r_{\mathrm{cut}} = 2.44$ Å	$r_{\mathrm{cut}} = 2.75$ Å	r_{TiO} (Å)
Melt		5.0(2)		1.881(5)
This paper	2.55	4.71	5.17	1.87
Modified Teter	4.56	4.68	4.98	1.86
Pedone	6.07	4.40	4.71	1.82
MA	5.82	4.35	4.89	1.92
EPSR	0.54	4.82	5.30	1.87
Rutile measured		5.7(2)[a]	5.7(2)[a]	1.962(5)
Rutile ideal		6.00	6.00	1.959

[a] From peak fit, not integration.

based on bond valence, assuming five equivalent bonds (of 1.898 Å), and neglecting any thermal expansion of the bonds at high temperature. Figure 3(b) demonstrates the efficacy of the high energy x-ray diffraction technique employed by comparing $T(r)$ measured for the recovered rutile material to that simulated based on the long-range averaged structure (known unit cell). Thermal broadenings (which do not follow from the crystallographic thermal parameters due to possible correlated motion at short range) were adjusted to be similar to the measurements ($\langle u^2_{\mathrm{TiO}}\rangle^{1/2} = 0.100$ Å, $\langle u^2_{\mathrm{OO}}\rangle^{1/2} = 0.072$ Å, $\langle u^2_{\mathrm{TiTi}}\rangle^{1/2} = 0.116$ Å). Direct peak fitting to the Ti-O peak yielded the position $r_{\mathrm{TiO}} = 1.962(5)$ Å and $n_{\mathrm{TiO}} = 5.7(2)$, the latter being 4% smaller than the expected value, and a measure of the overall uncertainty of coordination numbers determined from both solid and liquid phase datasets. Table II summarizes the pertinent values obtained.

A key finding of the MD modeling study was that, in the *NPT* ensemble, all of the preexisting potential models tested would drive the system towards a density much lower than expected from the experimental measurements [39] (Table I). As discussed above, the potentials of this paper and the modified Teter potentials were adjusted in order to give the expected density at 2250 K. Figure 1 compares the densities obtained with these two sets of potentials over a wide temperature range, where they show excellent agreement with experimental data, including that for the densest (lowest porosity [17]) amorphous TiO_2 films at room temperature. Figure 4 compares the experimentally weighted model interference functions directly with the experimental data. By construction, the EPSR model gives an excellent fit, while all of the preexisting MD models predict sharper features in the structure factor than those observed in the measured data. It was for this reason that we chose to derive a new set of potentials, in order to better simulate the measured liquid structure factor. We note that the potentials derived by EPSR may also be used for MD, but that they take a more cumbersome analytical form (the empirical terms comprise a sum of Poisson curves), or may be used in numerical form. Quantitative comparison of the models is made with reference to the real-space functions shown in Fig. 5 and using the quality-of-fit parameter [54]

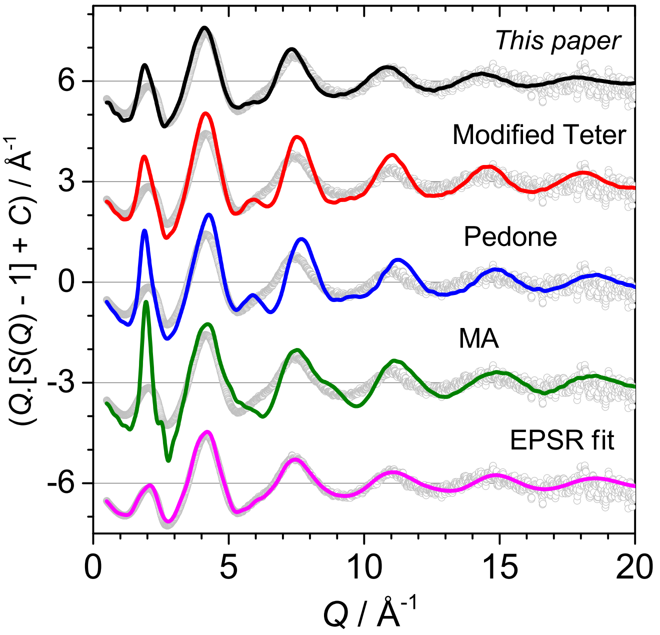

FIG. 4. (Color online) Interference functions $Q[S(Q) - 1]$ for various MD models (solid curves) obtained using the potentials of this work (*NPT*), Teter (modified, *NPT*), Pedone [48] (*NVT*), MA [46] (*NVT*), compared to the experimental data (open points). A model derived by EPSR to the measured x-ray structure factor is also shown. Vertical offsets C have been applied for clarity.

$$R_{\chi}(r_{k,\max}) = \left\{ \frac{\sum_{k=1}^{k,\max} [T_{\mathrm{exp}}(r_k) - T_{\mathrm{mod}}(r_k)]^2}{\sum_{k=1}^{k,\max} T^2_{\mathrm{exp}}(r_k)} \right\}^{1/2}, \qquad (7)$$

where subscripts exp and mod denote experimental and modeled functions, respectively. The $R\chi$ calculated for each model ($1.2 \leqslant r_k \leqslant 10.0$ Å) are recorded in Table II, showing that those of this paper are the best, by this measure. The dependence of $R\chi$ on the maximum cutoff distance $r_{k,\max}$ is shown in Fig. 6. Both the MA [46] and the Pedone [48] potentials give rise to total x-ray $T(r)$ functions (Fig. 5) which are overstructured at high r, while the like and unlike pair functions $t_{ij}(r)$ derived using the modified Teter and potentials of this paper are in antiphase and of sufficient amplitude, so as to reproduce the rather flat and featureless $T(r)$ measured experimentally for $r > 5$ Å. Furthermore, Table II shows that the MA [46] and Pedone [48] potentials respectively over- and underestimate the peak Ti-O bond length. For each model, coordination numbers n_{TiO} obtained from the Ti-O partial radial distribution functions $4\pi\rho c_{\mathrm{O}} r^2 g_{\mathrm{TiO}}(r)$ fall below the value 5.0(2) determined directly from the diffraction data (cutoff 2.44 Å, Table II). According to most of the models, this is partly due to the inclusion of intensity from the O-O partial in the experimentally determined value.

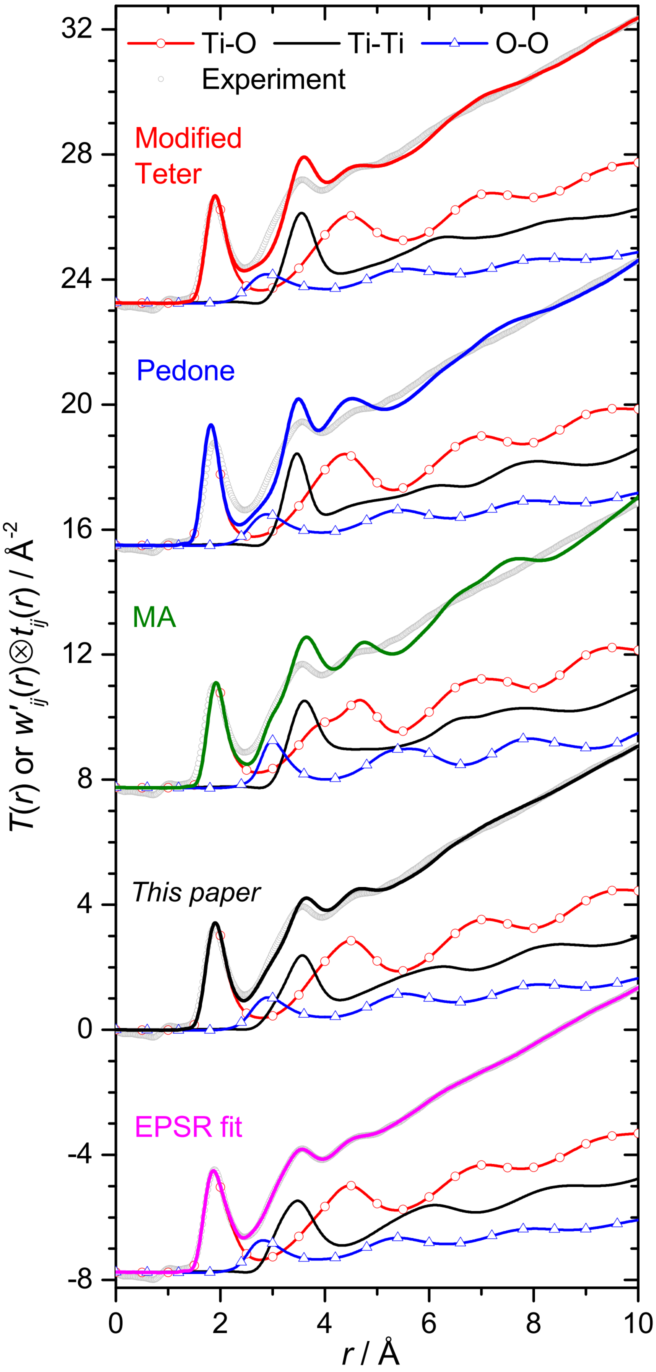

FIG. 5. (Color online) Comparison of experimental $T(r)$ (open points) to those from MD modeling and EPSR, Fourier transformed from the interference functions shown in Fig. 4. Also shown are the x-ray weighted partial correlation functions $w'_{ij}(r) \otimes t_{ij}(r)$ where $w'_{ij}(r)$ are the Fourier transforms of the $W_{ij}(Q)$ [Eq. (3)] and $\otimes$ denotes convolution. Vertical offsets have been used for clarity.

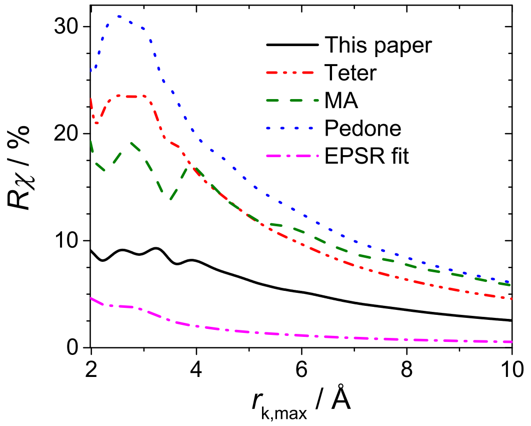

FIG. 6. (Color online) Dependence of the quality-of-fit parameter $R\chi$ [Eq. (7)] on the upper cutoff distance $r_{k,\max}$ for the five molten TiO_2 models considered (see Fig. 5 and Table II).

V. DISCUSSION

A. Densities of liquid, amorphous, and crystalline TiO_2

Extrapolating the thermal expansion trend for rutile measured by Henderson *et al.* [55], the density at the melting point (2135 K) is $4.04\,\mathrm{g\,cm^{-3}}$, while interpolating for the liquid trend from Dingwell [39], the density is $3.24\,\mathrm{g\,cm^{-3}}$, giving a large density drop of 20% on melting [or 25% increase on crystallization, Fig. 1(a)]. This is of very similar magnitude to that observed for the corundum → liquid Al_2O_3 [28] and quartz → liquid SiO_2 [56] transitions. The SiO_2 melting transition is not accompanied by a change in coordination number [56,57], but the Al_2O_3 melting is (where n_{AlO} drops from 6.0 to 4.4 [28]). This has been attributed by Skinner *et al.* [26] essentially to the higher field strength of Si^{4+}. Our finding that n_{TiO} drops on melting is consistent with this picture based on the similar field strengths of Ti^{4+} and Al^{3+}.

The structure of liquid TiO_2 has previously been simulated by Hoang [44,45] using MD and the potentials of MA [46]. These were however conducted at fixed densities, independent of temperature, with the lowest liquid density used $3.80\,\mathrm{g\,cm^{-3}}$, corresponding to that of dense amorphous TiO_2 films [17] and much higher than the measured values [39] for the liquid. The structure and properties thus derived are therefore more pertinent to the *high pressure* liquid, where both density and coordination numbers would be higher. With the slight modifications made in this paper to the Teter potentials, we were able to obtain the expected density (based on [39]) at 2250 K, and using these potentials, we estimate that the high liquid density of $3.80\,\mathrm{g\,cm^{-3}}$ used by Hoang [44,45] corresponds to a pressure of 4.8 GPa (note that the *model* pressure using the MA potentials would be much higher: 65 GPa at 2250 K and $3.21\,\mathrm{g\,cm^{-3}}$). Both the modified Teter potentials and those of this paper allow for the prediction of the density $\rho(T)$ over a wide range of temperatures, over much of the experimentally stable liquid region, and through supercooling to form glassy TiO_2. Both the experimentally determined thermal expansion of the liquid [39] and the density of the amorphous phase are reproduced by our models, Fig. 1. The experimental densities of amorphous TiO_2 films vary greatly [17], although those with lower density typically have higher porosity, and we naturally expect dense, pore-free models to be close to the upper end of the experimental values, as found [Fig. 1(a)]. The slightly lower density of our models compared to the upper bound of experimental amorphous TiO_2 densities may be a result of the rapid quenching necessary in MD simulations, which is supported by the comparison between models cooled at $4 \times 10^{12}\,\mathrm{K\,s^{-1}}$ [blue diamond, Fig. 1(a),

TABLE III. Volume thermal expansion coefficients α_V [Eq. (8)] derived from MD simulations of liquid and amorphous TiO_2 compared to measured values for the melt [39] and crystalline rutile TiO_2 [55]. All α_V are referenced to $T_R = 298$ K, and the columns ΔT indicate the range over which α_V was calculated. Glass transition temperatures derived from the model potential energy, after Micoulaut *et al.* [64] are also given, as are the T coefficients of n_{TiO} in the melt dn_{TiO}/dT.

	Volume thermal expansion coefficient α_V (10^{-6} K^{-1})							
	Melt	ΔT (K)	Amorphous	ΔT (K)	Rutile	ΔT (K)	T_g (K)	dn_{TiO}/dT (10^{-4} K^{-1})
MD *this paper*	81.8(7)	1898–2798	30.39(2)	298–898			950(110)	– 3.0(1)
MD modified Teter	70.3(7)	1873–2743	27.98(2)	298–1198			1330(110)	– 1.7(1)
Measured	89.0 [39]	1873–2198			27.35 [55]	296–1578		

$T = 298$ K] and at 100×10^{12} Ks^{-1} [open orange square, Fig. 1(a), $T = 298$ K], the larger rate resulting in a 3% decrease in density. First principles MD models of amorphous TiO_2 have been obtained [58] with densities of 3.56 to 3.59 g cm^{-3}; essentially the same as that found here [3.57(1) g cm^{-3}].

If fixed density simulations are to be performed, then the importance of the choice of density parameter, when modeling any condensed phase, cannot be underestimated. This is clear, for example, from the strong dependence of n_{TiO} on density in models of liquid and amorphous TiO_2 [44,45,59,60], and from Discussion Sec. V B–D. The advantage of models capable of predicting density, such as those used here, is therefore significant.

B. Thermal expansion

The volume thermal expansion coefficients α_V can be calculated from the variation in density with temperature $\rho(T)$ using

$$\alpha_V = \left[\frac{\rho(T_R)}{\rho(T)} - 1\right]\frac{1}{\Delta T} = \frac{1}{V(T_R)}\left(\frac{\Delta V}{\Delta T}\right), \tag{8}$$

where Δ denotes a difference in density $\Delta\rho = \rho(T_R) - \rho(T)$, volume $\Delta V = V(T) - V(T_R)$, or temperature $\Delta T = T - T_R$, and $T_R = 298$ K is a chosen reference temperature. Table III records the modeled α_V over the linear expansion regions, where it can be seen that the modeled amorphous phase TiO_2 shows very similar, though slightly larger, expansion compared to rutile TiO_2 [55]. For the liquid phase, the modeled α_V are much larger than for the solid phases, and smaller than that derived from Dingwell's measurements [39] on the melt, by 8% in the case of the improved potentials of this paper, and 21% for the Teter potentials. The origin of the discrepancies is not clear, but it should be noted that the experimental value is based on only two density measurements plus one extrapolated point from $CaSiO_3$-TiO_2 pseudobinary melts, and covers a smaller temperature range (Table III) than the modeled values. The large α_V of the melt is due in part to temperature dependent structural changes (discussed in Sec. V D).

It is remarkable that Henderson *et al.* [55] have shown that the thermal expansion of the two longer, axial Ti-O bonds within the $[TiO_6]$ octahedron of rutile TiO_2 is more than seven times larger than that of the four shorter, equatorial bonds. This can be considered as a precursory effect to the reduction of the average n_{TiO} upon melting, from six to about five in the melt.

C. Local structure of liquid TiO_2

The $t_{ij}(r)$ of the EPSR, MD (this paper), and three literature MD models (Fig. 5) show some significant differences and similarities. For example, the $t_{\mathrm{OO}}(r)$ are mostly very similar, except for that of the MA MD model, which is much sharper. Indeed, while of the three literature MD models, the first (Ti-O) peak of the MA model reproduces the experimental data most closely (Figs. 5 and 6), at higher r, the $t_{\mathrm{TiO}}(r)$ is the most different from the other models, showing a pronounced shoulder of the second Ti-O peak at about 4.0 Å. The oversharpness of the $t_{ij}(r)$ peaks in the liquid TiO_2 models obtained using the literature potentials is related to their high melting points in the rutile phase. These were all found to be >2843 K and much greater in the case of the MA potentials, and hence much greater than the experimental melting point of 2135 K. In deriving the potentials of this paper (Table I) and obtaining an improved simulation of the melt structure, the model rutile melting point was incidentally also reduced toward the experimental value, but remaining higher at about 2470(80) K.

The structural characteristics of both the EPSR and best MD model were investigated in more detail. The average coordination numbers n_{TiO} and $n_{\mathrm{OTi}} = (1/2)n_{\mathrm{TiO}}$ are broken down into their distributions in Fig. 7(a). The majority species are fivefold $[TiO_5]$ polyhedra, having around 50% abundance, with the remaining Ti being either fourfold or sixfold, with slightly more of the latter [cutoff dependent, Fig. 7(b)]. Given the average n_{TiO} of about five (Table II), the average n_{OTi} is about 2.5, with about half of the oxygen atoms bonded to two Ti, in bridging-oxygen-like environments, and the other half to three Ti in crystalline-TiO_2-like local environments. This implies a large degree of corner sharing, as well as edge sharing, between $[TiO_m]$ polyhedra. This fact is also manifest in the asymmetry of the first peak in the $t_{\mathrm{TiTi}}(r)$, which in the amorphous phase at room temperature is resolved into two separate Ti-Ti peaks in our model. Such splitting of the Ti-Ti peak has been observed previously [20,45,58] in amorphous TiO_2. Figure 7(c) shows bond angle distributions (BADs) for the EPSR and MD models (this paper), where again there is broad qualitative agreement and some quantitative differences. The partial BADs (not shown) reveal that the various polyhedra are not overly distorted, for example, the fourfold $[TiO_4]$ are tetrahedral with mean O-Ti-O angle of 109.1°.

D. Temperature dependence of the liquid structure

The temperature dependence of the average coordination numbers derived using the new MD potentials are shown in

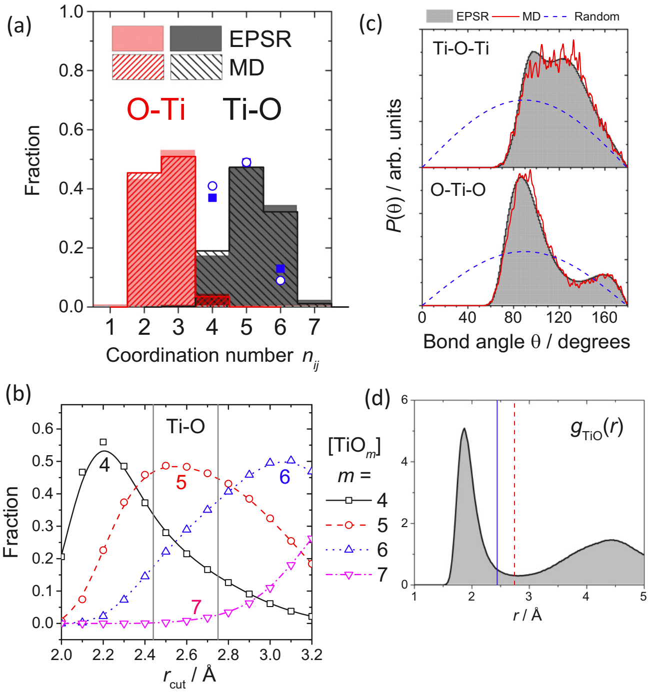

FIG. 7. (Color online) (a) and (b) Coordination number and (c) BADs calculated for the EPSR and MD models (this paper) of molten TiO_2 at 2243 K. The cutoff distance for Ti-O separations used in (a) and (c) was 2.75 Å, while (b) shows the dependence of the Ti-O coordination number distribution on cutoff distance r_{cut} for the EPSR model; lines are guides to the eye. Vertical lines correspond to cutoffs used to calculate the averages in Table II, and these are also compared to $g_{TiO}(r)$ in (d). Si-O coordination number distributions for high pressure liquid silica are shown for comparison in (a) as closed blue squares (*ab initio* MD [67], 3500 K, 27 GPa) and open blue circles (*ab initio* MD [68], 3000 K, 20 GPa).

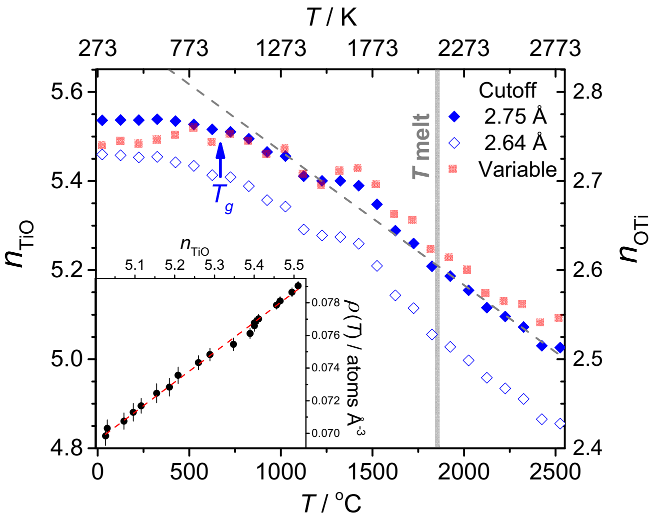

FIG. 8. (Color online) Average coordination numbers of liquid and amorphous TiO_2 obtained by MD modeling using the potentials of this paper; the glass transition temperature is indicated as T_g. Values for two fixed cutoffs and for a variable cutoff set at the minimum of $g_{TiO}(r)$. The right-hand ordinate axis shows $n_{OTi} = (1/2)n_{TiO}$. The dashed line is a fit to the equilibrium liquid data, and its extrapolation to lower temperatures, and is given by $n_{TiO} = 5.8497 - (3.00625 \times 10^{-4})T$ (in K). Inset shows number density $\rho(T)$ as a function of n_{TiO} (2.75 Å cutoff), with the dashed (red) line a least squares fit. The cutoffs for the variable cutoff points (light red squares) were determined by fourth-order polynomial fits to $g_{TiO}(r)$ in the region $2.26 < r < 3.40$ Å.

Fig. 8. It is clear that the liquid structure is in fact weakly temperature dependent, the average coordination numbers displaying a gradual decline with increasing temperature. A fit to the liquid data up to 2798 K yields a temperature coefficient of $-3.0(1) \times 10^{-4}$ K^{-1} for n_{TiO} (dashed line in Fig. 8, full precision trend given in Fig. 8 caption, see also Table III), equivalent to $-5.8(2) \times 10^{-3}$% K^{-1} compared to the values at the melting point, for both Ti-O and O-Ti coordination numbers. Hence over the whole range of liquid stability, which is of order 10^3 K, the n_{ij} are expected to change by only about 6%.

Melt fragility measures the degree of deviation from Arrhenian behavior of the liquid viscosity and has been directly related to the temperature dependence of the number of degrees of freedom per atom [61–63]. Hence the observed temperature dependence of the coordination numbers is expected to contribute to an increased liquid fragility, as well as to the large thermal expansion coefficient (see Table III and Fig. 1). The authors are not aware of any viscosity measurements on pure TiO_2 melts.

Below the melting point, in the supercooled liquid region, the points in Fig. 8 deviate from linearity and from the extrapolated trend shown by the dashed line. This is related to the fact that the system densities (Fig. 1) also deviate from a smooth trend in this region, and the inset to Fig. 8 shows the strong correlation between density and n_{TiO}. Taking into account the temperature dependence of the position of the first minimum in $g_{TiO}(r)$ to define the coordination numbers (light red squares, Fig. 8) does not remove the deviation. We attribute the deviations in density and the n_{ij} to the sensitivity of the simulations to finite size and timescale effects in the high viscosity, supercooled liquid region, as discussed by Micoulaut *et al.* [64]. Using the variable cutoff trend (Fig. 8), the difference between n_{TiO} for the liquid at the melting point and amorphous TiO_2 at room temperature is 0.23, or 4.3%, which is smaller than the 6.0% indicated by the trend obtained using a fixed cutoff of 2.75 Å to define n_{TiO}.

The strong correlation between liquid density and structure is characterized by the gradient $d\rho/dn_{TiO} = 0.0183(3)$ atoms Å^{-3} (see Fig. 8 inset), derived by combining the data of Figs. 1 and 8. This value is in agreement with that predicted by fixed density *ab initio* MD simulations of amorphous TiO_2 {0.0173(5) Å^{-3} [59]}.

We have determined the hypothetical glass transition temperature from our MD models using the discontinuity in the model potential energy, after Micoulaut *et al.* [64], Table III. Using the modified Teter potentials, a value comparable to the T_g determined by Hoang [44,45] using MD with the MA potentials, at higher (fixed) densities of 3.80 to 4.20 g cm^{-3}, is obtained, while a lower value is obtained using the potentials of this paper. Due to the lack of an experimentally observed glass transition, it is difficult to comment on the relative merits of each prediction. During experiments, we rarely observed supercooling of the melt owing to the existence of a top-to-bottom temperature gradient and the presence of small crystallites in the bottom of the sample, well away from the laser heated liquid upper region probed by x-ray diffraction and pyrometry. This compromise was accepted because, upon full melting of the sample, it would tend to destabilize and adhere to the nozzle such that the experiment had to be terminated. On one occasion during later testing, a stable melt was obtained, and supercooling was observed down to the onset of recalescence at 1580 K. Hence it is possible that the theoretical glass transition temperatures are testable if the cooling rate can be increased above the observed 177(2) K s^{-1} (at 1580 K).

E. Comparison to high pressure liquid SiO_2

It is well known that crystalline TiO_2 represents an analog to SiO_2 at higher pressures [21]. Indeed, as pressure is applied to quartz SiO_2, it transforms first to coesite and then to stishovite, which is stable above about 8.7 GPa. Stishovite has the rutile structure, which is the most common naturally occurring structure for TiO_2.

Given the above, we investigate the extension of this analogy to the liquid state. Liquid TiO_2 at ambient pressure has an average n_{TiO} close to five, while liquid silica has $n_{\mathrm{SiO}} = 4$ [56,57]. However, as pressure is increased, it has been shown both experimentally for SiO_2 glass [65,66] and computationally for SiO_2 liquid [67,68] that the average Si-O coordination increases. We can therefore estimate the pressure of the analogous SiO_2 melt as that at which silicon is fivefold coordinated to oxygen. In the glass, this is at about 27 GPa [65,66], and is comparable to existing *ab initio* calculations for the melt at 3500 K and 27 GPa [67] ($n_{\mathrm{SiO}} = 4.76$) or 3000 K and 20 GPa [68] ($n_{\mathrm{SiO}} = 4.68$). Such pressures for the liquid correspond to molten stishovite, being well above the equilibrium phase fields for quartz and coesite. Calculated coordination number distributions for molten silica are compared to those for TiO_2 in Fig. 7(a), showing some similarity, although the comparison is rather qualitative given the mismatches in average coordination number (owing to the availability of liquid silica data only at discreet pressure values [67,68]). Figure 9 compares the measured x-ray structure factors for ambient pressure liquid titania and silica glass at 27 GPa. Despite small differences in x-ray scattering weighting factors and the large temperature difference, the two functions show considerable similarity, plotted using the dimensionless quantity $r_1 Q$, with r_1 the nearest neighbor bond length taken from the measured $T(r)$.

We note that GeO_2 represents a further analog to the TiO_2 and SiO_2 melts, with germania glass having an average Ge-O coordination number of five at intermediate pressure, determined by various authors to be about 14.5 GPa [69] (neutron diffraction), 10.5 GPa [70] (x-ray diffraction), or 11 GPa [64] (classical MD). Indeed, it is likely that the melts of $HfO_2 \rightarrow ZrO_2 \rightarrow TiO_2 \rightarrow GeO_2 \rightarrow SiO_2$ form a series of structural analogs at increasing pressures, from left to right, and potentially with other oxides based on tetravalent cations such as Sn, Pb, U, Th, etc., where the various pressures for isomorphic liquid pairs remain to be determined. For example, molten ZrO_2 at ambient pressure has $n_{\mathrm{ZrO}} = 6.1(4)$ [26], a coordination number that would be obtained in molten TiO_2 only at elevated pressures. This is comparable to the crystalline state where rutile TiO_2 transforms at 12 GPa [71] into a phase isomorphous with ambient baddeleyite ZrO_2, with sevenfold cations.

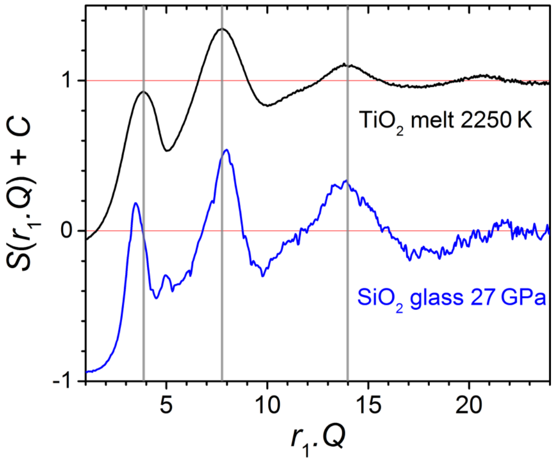

FIG. 9. (Color online) Comparison of the x-ray structure factors for liquid TiO_2 and room temperature SiO_2 glass at 27 GPa [66] plotted as functions of the dimensionless coordinate $r_1 Q$, where r_1 is the peak Ti-O or Si-O bond length as measured in the Fourier transforms of the respective $S(Q) - 1$.

F. TiO_2 polymorphs with low Ti-O coordination

Given the stable existence of fivefold as well as fourfold coordinated titanium in liquid TiO_2, as well as in several complex crystalline and glassy titanates, it is natural to speculate on the existence of metastable crystalline TiO_2 polymorphs containing Ti with a coordination number less than six, in contrast to the majority of known ambient pressure polymorphs [21,72]. In fact, recent refinements of diffraction data and density functional theoretic calculations [23] have been used to show that the TiO_2(B) polymorph can be considered as having $n_{\mathrm{TiO}} = 5.5$, being composed of equal numbers of sixfold and fivefold Ti polyhedra with the latter having one additional long, very weak bond. Moreover, monolayer nanosheets of this polymorph can be composed entirely of fivefold Ti [73–75].

It is interesting to note that Lacks and Gordon [76] have shown, using a polarization-included electron-gas model, that TiO_2 placed in the quartz structure (fourfold $[TiO_4]$ tetrahedra) at ambient pressure is metastable and relaxes toward a higher pressure version of the quartz SiO_2 structure with reduced X-O-X bond angles. Furthermore, Lacks and Gordon [76] found quartz TiO_2 to be *stable*, relative to the rutile form, at a negative pressure of −5 GPa. Hypothetical coesite TiO_2 (also built from fourfold $[TiO_4]$ tetrahedra) could therefore be expected to be stable at more modest negative pressures, given that it is the silica polymorph stable at pressures intermediate between the quartz and stishovite phase fields, and also to be metastable at ambient pressure (although no such phase is observed for GeO_2). Very recently, TiO_2 in the tridymite structure (a high T polymorphic form of SiO_2, also containing tetrahedral cations) has also been shown to be metastable at ambient pressure [77], but what of hypothetical TiO_2 structures built from fivefold [TiO_5] polyhedra or with mixed Ti coordination states? Such structures should also be expected to be metastable with respect to rutile, but even closer in free energy and density to the aforementioned compared to the fourfold structures. MO_2 structures based entirely on [MO_5] polyhedra are very rare. We are aware only of a vanadium dioxide polymorph VO_2(C), which is a layered compound composed of sheets of [VO_5] square pyramids [78,79], although full crystallographic data have not been published, possibly due to nonstoichiometry and the retention of Li or H_2O from the synthesis route.

There are other reasons for considering the existence of energetically competitive TiO_2 polymorphs based on Ti coordination polyhedra with fewer than six ligands. The semiempirical model of ideal associated solutions (IAS) [80] is used to predict the chemical structure of liquids and glasses based on the law of mass action and the free energies of the stoichiometric compounds within a given phase diagram (e.g., pseudobinary MO_x-JO_y), as functions of T, P, and composition. The IAS model has been applied successfully to model various properties of glasses at room temperature [80] as well as to predict variation of coordination numbers in oxide melts as a function of T [81,82]. Typically, however, only high temperature polymorphs of congruently melting stoichiometries are considered. This means that, for end-member oxides, such as TiO_2, no change in coordination number between high temperature stable crystalline phase (rutile) and melt is predicted, in contrast to the experimental observations of this paper. The standard IAS model is therefore not applicable to many single oxide systems, such as TiO_2 and Al_2O_3, as well as to TiO_2- or Al_2O_3-rich multicomponent systems, to name but a few examples where differences between crystal and melt (or glass) cation-oxygen coordination number have been observed and recently reviewed [26].

In a binary oxide melt, the standard IAS model can be used to predict the fractions of various stoichiometric groupings, which exist locally within the liquid. Thus the model implicitly relies upon local compositional fluctuations which are expected to occur in the melt. In a single oxide liquid, no such local compositional fluctuations are expected, but local density fluctuations may still occur, and these are associated not with other possible stoichiometries, but with other possible polymorphs, which are sampled locally as regions of the melt explore the underlying energy landscape. This is qualitatively similar to the concept of polymorphoids expounded by Minaev *et al.* [83], and related phenomenology is important in the concepts of polyamorphism and liquid-liquid phase transitions [84].

Therefore, considering a modified IAS model, where not only high temperature stable, but all energetically competitive polymorphs are included, the low cation-oxygen coordination observed in liquid TiO_2 in this paper and for various other oxide melts and glasses [26] implies, at least in the case of single oxide systems, the existence of energetically competitive crystalline polymorphs, also with cation-oxygen coordination numbers lower than for the high temperature stable phase. Comparison can be made to the Al_2O_3 system, in which molten alumina has $n_{\mathrm{AlO}} = 4.4$ [28]; the stable crystal polymorph corundum has $n_{\mathrm{AlO}} = 6.0$, but several metastable polymorphs exist (such as γ-Al_2O_3) with mixed tetrahedral-octahedral coordination [30] and, on average, $4 < n_{\mathrm{AlO}} < 6$.

We suggest that experimental and theoretical searches for low-coordinated materials, such as TiO_2 based on fivefold Ti-O polyhedra, may prove fruitful. These are expected to have lower densities than the more highly coordinated structures, such as the sixfold rutile phase, but higher or similar densities to the microporous ramsdellite (R) and TiO_2(B) and mesoporous hollandite (H) TiO_2 polymorphs [see Fig. 1(a)], the latter of which is even less dense than amorphous TiO_2, Fig. 1(a). Evolutionary crystal structure prediction has been applied to the TiO_2 system previously [85], but in that case, the search was intentionally biased towards materials with high hardness, which turned out to be composed of sevenfold or sixfold Ti, similar to the known high pressure phases of TiO_2.

VI. CONCLUSIONS

High energy x-ray diffraction measurements on molten TiO_2 have revealed an average Ti-O coordination number close to 5.0(2). The MD and EPSR models that are in the best agreement with the diffraction data suggest that the structure is based on lower coordination polyhedra (mainly fivefold [TiO_5]) than the vast majority of the known crystalline polymorphs, which contain only octahedral titanium at ambient pressure. This finding is in qualitative accord with a recently observed trend [26] for oxide melts, toward lower-than-crystal coordination numbers, with the effect being larger for lower field strength cations.

We have obtained classical MD potentials which reproduce the structure of molten TiO_2 better than any other published potentials. In addition, our potentials are able to reproduce the liquid and amorphous state densities and thermal expansions of TiO_2, in agreement with literature data. This is of critical importance given the strong correlation between density and structural parameters such as n_{TiO}. An associated prediction is a weakly temperature dependent liquid structure, which contributes to the large thermal expansion of the melt.

We argue on the basis of our result that metastable polymorphs of TiO_2, based on lower-than-octahedral Ti-O polyhedra, may yet be obtained, either experimentally and/or computationally. This is somewhat in analogy to the known polymorphism and liquid structure of alumina.

Liquid titania represents a structural analog to molten silica at higher pressure, estimated to be in the region of 27 GPa. As such, the study of more complex titanate melts may well open a window on the structure and properties of geologically relevant silicate melts at high pressure.

ACKNOWLEDGMENTS

Use of the Advanced Photon Source, an Office of Science User Facility operated for the US Department of Energy (DOE) Office of Science by Argonne National Laboratory, was supported by the US DOE under Contract No. DE-AC02-06CH11357. O.L.G.A. (wrote paper, MD simulations, experiment), J.K.R.W. (experiment, manuscript preparation), A.T. (experiment), and C.J.B. (experiment, manuscript preparation) were supported by US DOE Grant No. DE-SC0007564 and L.B.S. (partial support of MD simulations, experiment, manuscript preparation) by US DOE, office of Basic Energy Sciences (BES) under contract number BES DE-FG02-09ER46650. We thank the anonymous referees for their constructive comments which led to numerous improvements to the manuscript.

[1] A. Fujishima, T. N. Rao, and D. A. Tryk, J. Photochem. Photobiol. C **1**, 1 (2000).

[2] U. I. Gaya and A. H. Abdullah, J. Photochem. Photobiol. C **9**, 1 (2008).

[3] M. Cologna, J. S. C. Francis, and R. Raj, J. Eur. Ceram. Soc. **31**, 2827 (2011).

[4] J. Narayan, Scripta Mater. **69**, 107 (2013).

[5] R. Raj, J. Eur. Ceram. Soc. **32**, 2293 (2012).

[6] S. John Paul, J. J. Yang, M. Ruth, S. Andreas, M.-R. Gilberto, R. S. Duncan, and R. S. Williams, Nanotechnology **20**, 485701 (2009).

[7] D. B. Strukov, G. S. Snider, D. R. Stewart, and R. S. Williams, Nature **453**, 80 (2008).

[8] D.-H. Kwon, K. M. Kim, J. H. Jang, J. M. Jeon, M. H. Lee, G. H. Kim, X.-S. Li, G.-S. Park, B. Lee, and S. Han, Nat. Nanotechnol. **5**, 148 (2010).

[9] J. J. Yang, D. B. Strukov, and D. R. Stewart, Nat. Nanotechnol. **8**, 13 (2013).

[10] J. M. Knaup, J. Marx, and T. Frauenheim, Phys. Status Solidi RRL **8**, 549 (2014).

[11] G. Handfield and G. G. Charette, Can. Metall. Quart. **10**, 235 (1971).

[12] D. R. Sadoway, J. Mater. Res. **10**, 487 (1995).

[13] N. A. Fried, K. G. Rhoads, and D. R. Sadoway, Electrochim. Acta **46**, 3351 (2001).

[14] A. Masuno, H. Inoue, J. Yu, and Y. Arai, J. Appl. Phys. **108**, 063520 (2010).

[15] S. D. Stookey, Ind. Eng. Chem. **51**, 805 (1959).

[16] G. Beall, Int. J. Appl. Glass. Sci. **5**, 93 (2014).

[17] D. Mergel, D. Buschendorf, S. Eggert, R. Grammes, and B. Samset, Thin Solid Films **371**, 218 (2000).

[18] J. Yu, S. Kohara, K. Itoh, S. Nozawa, S. Miyoshi, Y. Arai, A. Masuno, H. Taniguchi, M. Itoh, M. Takata, T. Fukunaga, S.-y. Koshihara, Y. Kuroiwa, and S. Yoda, Chem. Mater. **21**, 259 (2009).

[19] L. Cormier, P. H. Gaskell, G. Calas, and A. K. Soper, Phys. Rev. B **58**, 11322 (1998).

[20] V. Petkov, G. Holzhüter, U. Tröge, T. Gerber, and B. Himmel, J. Non-Cryst. Solids **231**, 17 (1998).

[21] Z. Fu, Y. Liang, S. Wang, and Z. Zhong, Phys. Status Solidi B **250**, 2206 (2013).

[22] Y. Le Page and P. Strobel, J. Solid State Chem. **44**, 273 (1982).

[23] M. B. Yahia, F. Lemoigno, T. Beuvier, J.-S. Filhol, M. Richard-Plouet, L. Brohan, and M.-L. Doublet, J. Chem. Phys. **130**, 204501 (2009).

[24] J. Gunter and G. Jameson, Acta Crystallogr. C **40**, 207 (1984).

[25] K. K. Wu and I. Brown, Acta Crystallogr. B **29**, 2009 (1973).

[26] L. B. Skinner, C. J. Benmore, J. K. R. Weber, J. Du, J. Neuefeind, S. K. Tumber, and J. B. Parise, Phys. Rev. Lett. **112**, 157801 (2014).

[27] S. Ansell, S. Krishnan, J. K. R. Weber, J. J. Felten, P. C. Nordine, M. A. Beno, D. L. Price, and M.-L. Saboungi, Phys. Rev. Lett. **78**, 464 (1997).

[28] L. B. Skinner, A. C. Barnes, P. S. Salmon, L. Hennet, H. E. Fischer, C. J. Benmore, S. Kohara, J. K. R. Weber, A. Bytchkov, M. C. Wilding, J. B. Parise, T. O. Farmer, I. Pozdnyakova, S. K. Tumber, and K. Ohara, Phys. Rev. B **87**, 024201 (2013).

[29] C. Landron, L. Hennet, T. E. Jenkins, G. N. Greaves, J. P. Coutures, and A. K. Soper, Phys. Rev. Lett. **86**, 4839 (2001).

[30] I. Levin and D. Brandon, J. Am. Ceram. Soc. **81**, 1995 (1998).

[31] D. A. Keen, J. Appl. Cryst. **34**, 172 (2001).

[32] E. Lorch, J. Phys. C **2**, 229 (1969).

[33] U. Rütt, M. A. Beno, J. Strempfer, G. Jennings, C. Kurtz, and P. A. Montano, Nucl. Instrum. Meth. A **467**(Part 2), 1026 (2001).

[34] J. K. R. Weber, S. Krishnan, C. D. Anderson, and P. C. Nordine, J. Am. Ceram. Soc. **78**, 583 (1995).

[35] L. B. Skinner, C. J. Benmore, and J. B. Parise, Nucl. Instrum. Meth. A **662**, 61 (2012).

[36] J. K. R. Weber, J. J. Felten, and P. C. Nordine, Rev. Sci. Instrum. **67**, 522 (1996).

[37] X. Qiu, J. W. Thompson, and S. J. L. Billinge, J. Appl. Cryst. **37**, 678 (2004).

[38] A. K. Soper and E. R. Barney, J. Appl. Cryst. **44**, 714 (2011).

[39] D. B. Dingwell, J. Am. Ceram. Soc. **74**, 2718 (1991).

[40] D. B. Dingwell, Geochim. Cosmochim. Ac. **56**, 3403 (1992).

[41] A. K. Soper, Phys. Rev. B **72**, 104204 (2005).

[42] O. L. G. Alderman, A. C. Hannon, D. Holland, S. Feller, G. Lehr, A. J. Vitale, U. Hoppe, M. Von Zimmermann, and A. Watenphul, Phys. Chem. Chem. Phys. **15**, 8506 (2013).

[43] W. Smith and T. R. Forester, J. Mol. Graphics **14**, 136 (1996).

[44] V. V. Hoang, J. Phys.: Condens. Matter **19**, 416109 (2007).

[45] V. V. Hoang, Phys. Status Solidi B **244**, 1280 (2007).

[46] M. Matsui and M. Akaogi, Mol. Sim. **6**, 239 (1991).

[47] D. R. Collins, W. Smith, N. M. Harrison, and T. R. Forester, J. Mater. Chem. **6**, 1385 (1996).

[48] A. Pedone, G. Malavasi, M. C. Menziani, A. N. Cormack, and U. Segre, J. Phys. Chem. B **110**, 11780 (2006).

[49] A. N. Cormack, J. Du, and T. R. Zeitler, Phys. Chem. Chem. Phys. **4**, 3193 (2002).

[50] J. Du and A. N. Cormack, J. Non-Cryst. Solids **349**, 66 (2004).

[51] C. J. Benmore, J. K. R. Weber, M. C. Wilding, J. Du, and J. B. Parise, Phys. Rev. B **82**, 224202 (2010).

[52] L. B. Skinner, C. J. Benmore, J. K. R. Weber, S. Tumber, L. Lazareva, J. Neuefeind, L. Santodonato, J. Du, and J. B. Parise, J. Phys. Chem. B **116**, 13439 (2012).

[53] H. le Roux and L. Glasser, J. Mater. Chem. **7**, 843 (1997).

[54] A. C. Wright, in *Experimental Techniques of Glass Science*, edited by C. J. Simmons and O. H. El-Bayoumi (The American Ceramic Society, Westerville, Ohio, 1993), p. 205.

[55] C. Henderson, K. Knight, and A. Lennie, Open Mineralogy Journal **3**, 1 (2009).

[56] L. B. Skinner, C. J. Benmore, J. K. R. Weber, M. C. Wilding, S. K. Tumber, and J. B. Parise, Phys. Chem. Chem. Phys. **15**, 8566 (2013).

[57] Q. Mei, C. J. Benmore, and J. K. R. Weber, Phys. Rev. Lett. **98**, 057802 (2007).

[58] B. Prasai, B. Cai, M. K. Underwood, J. P. Lewis, and D. Drabold, J. Mater. Sci. **47**, 7515 (2012).
[59] T. Köhler, M. Turowski, H. Ehlers, M. Landmann, D. Ristau, and T. Frauenheim, J. Phys. D: Appl. Phys. **46**, 325302 (2013).
[60] M. Landmann, T. Köhler, E. Rauls, T. Frauenheim, and W. G. Schmidt, J. Phys.: Condens. Matter **26**, 253201 (2014).
[61] G. G. Naumis, Phys. Rev. E **71**, 026114 (2005).
[62] J. C. Mauro, P. K. Gupta, and R. J. Loucks, J. Chem. Phys. **130**, 234503 (2009).
[63] P. K. Gupta and J. C. Mauro, J. Chem. Phys. **130**, 094503 (2009).
[64] M. Micoulaut, Y. Guissani, and B. Guillot, Phys. Rev. E **73**, 031504 (2006).
[65] T. Sato and N. Funamori, Phys. Rev. B **82**, 184102 (2010).
[66] C. J. Benmore, E. Soignard, S. A. Amin, M. Guthrie, S. D. Shastri, P. L. Lee, and J. L. Yarger, Phys. Rev. B **81**, 054105 (2010).
[67] A. Trave, P. Tangney, S. Scandolo, A. Pasquarello, and R. Car, Phys. Rev. Lett. **89**, 245504 (2002).
[68] B. B. Karki, D. Bhattarai, and L. Stixrude, Phys. Rev. B **76**, 104205 (2007).
[69] P. S. Salmon, J. W. E. Drewitt, D. A. J. Whittaker, A. Zeidler, K. Wezka, C. L. Bull, M. G. Tucker, M. C. Wilding, M. Guthrie, and D. Marrocchelli, J. Phys.: Condens. Matter **24**, 415102 (2012).
[70] Q. Mei, S. Sinogeikin, G. Shen, S. Amin, C. J. Benmore, and K. Ding, Phys. Rev. B **81**, 174113 (2010).
[71] L. Gerward and J. Staun Olsen, J. Appl. Cryst. **30**, 259 (1997).
[72] V. Swamy, J. D. Gale, and L. Dubrovinsky, J. Phys. Chem. Solids **62**, 887 (2001).
[73] A. Vittadini, F. Sedona, S. Agnoli, L. Artiglia, M. Casarin, G. A. Rizzi, M. Sambi, and G. Granozzi, ChemPhysChem **11**, 1550 (2010).
[74] A. Vittadini, M. Casarin, and A. Selloni, Theor. Chem. Acc. **117**, 663 (2007).
[75] F. De Angelis, C. Di Valentin, S. Fantacci, A. Vittadini, and A. Selloni, Chem. Rev., doi:10.1021/cr500055q.
[76] D. J. Lacks and R. G. Gordon, Phys. Rev. B **48**, 2889 (1993).
[77] T. Zhu and S.-P. Gao, J. Phys. Chem. C **118**, 11385 (2014).
[78] T. A. Chirayil, P. Y. Zavalij, and M. S. Whittingham, J. Electrochem. Soc. **143**, L193 (1996).
[79] D. Hagrman, J. Zubieta, C. J. Warren, L. M. Meyer, M. M. Treacy, and R. C. Haushalter, J. Solid State Chem. **138**, 178 (1998).
[80] B. A. Shakhmatkin, N. M. Vedishcheva, M. M. Shultz, and A. C. Wright, J. Non-Cryst. Solids **177**, 249 (1994).
[81] M. Liška, J. Macháček, P. Perichta, O. Gedeon, and J. Pilát, Ceram.-Silikáty **52**, 61 (2008).
[82] N. M. Vedishcheva, B. A. Shakhmatkin, and A. C. Wright, Phys. Chem. Glasses: Eur. J. Glass Sci. Technol. B **41**, 260 (2000).
[83] V. S. Minaev, S. P. Timoshenkov, and V. V. Kalugin, Phys. Status Solidi C **8**, 2701 (2011).
[84] P. F. Mcmillan, M. Wilson, M. C. Wilding, D. Daisenberger, M. Mezouar, and G. N. Greaves, J. Phys.: Condens. Matter **19**, 415101 (2007).
[85] A. O. Lyakhov and A. R. Oganov, Phys. Rev. B **84**, 092103 (2011).
[86] E. P. Meagher and G. A. Lager, Can. Mineral. **17**, 77 (1979).
[87] M. Horn, C. Schwerdtfeger, and E. Meagher, Z. Kristallogr. **136**, 273 (1972).
[88] J. Akimoto, Y. Gotoh, Y. Oosawa, N. Nonose, T. Kumagai, K. Aoki, and H. Takei, J. Solid State Chem. **113**, 27 (1994).
[89] R. Marchand, L. Brohan, and M. Tournoux, Mater. Res. Bull. **15**, 1129 (1980).
[90] M. Latroche, L. Brohan, R. Marchand, and M. Tournoux, J. Solid State Chem. **81**, 78 (1989).
[91] A. C. Hannon, Rutherford Appleton Laboratory Report, RAL-93-063, 1993.
[92] W. H. Baur, Acta Crystallogr. **9**, 515 (1956).